https://doi.org/10.2352/ISSN.2470-1173.2020.16.AVM-258

Active Stereo Vision for Precise Autonomous Vehicle Control

Michael Feller, Jae-Sang Hyun and Song Zhang; Purdue University, School of Mechanical Engineering; West Lafayette, Indiana

Abstract

This paper describes the development of a low-cost, low-power, accurate sensor designed for precise, feedback control of an autonomous vehicle to a hitch. The solution that has been developed uses an active stereo vision system, combining classical stereo vision with a low cost, low power laser speckle projection system, which solves the correspondence problem experienced by classic stereo vision sensors. A third camera is added to the sensor for texture mapping. A model test of the hitching problem was developed using an RC car and a target to represent a hitch. A control system is implemented to precisely control the vehicle to the hitch. The system can successfully control the vehicle from within 35⁰ of perpendicular to the hitch, to a final position with an overall standard deviation of 3.0 mm of lateral error and 1.5⁰ of angular error.

Introduction

In recent years, advancements in the development of autonomous vehicles have been a major area of study, with breakthroughs occurring regularly in many different industries. One particular problem that is very important for the advancement of autonomous vehicles is the hitching problem. The hitching problem is complex and requires sensing of a hitch and then controlling the vehicle to attach to that hitch. This problem is different from many other problems in autonomous vehicles, as precise, centimeter-level accuracy movement is crucial to successfully complete a hitching maneuver, whereas in maneuvers such as lane centering or harvesting in agriculture, for example, a lower threshold of accuracy is sufficient. As an additional challenge in many hitching applications, the sensor used for autonomous hitching must be able to work in close proximity with other sensors of the same type without interference.

While hitching is a significant problem to solve in the autonomous vehicle industry, surprisingly little academic research has been published presenting possible solutions to the problem. The primary study of the hitching problem to date used a laser range finder to control a tractor to autonomously hitch to an implement [1]. In this study, the researchers were able to control an autonomous tractor to the implement with a lateral error of 3 cm and an angular error of 2⁰. Since artificial reflectors are required for the technology to work, significant modifications would need to be made to implements for tractors to detect them. Furthermore, the sensing components used in this study are listed with model numbers, and upon investigation of the component specifications, it can be discovered that the system would cost thousands of dollars and use about 30 watts of power.

As has been established to the best knowledge of the present authors, there are currently no published or in production methods for autonomously hitching a vehicle that (a) do not require modification of the implement being hitched to, (b) incorporate sensors costing in total under $1000, or (c) use less than 20 watts of power. Furthermore, the state-of-the-art lacks consistency, and more robust development could improve upon the accuracy and consistency of present methods.

Stereo vision has been studied and is of significant importance in the development of computer vision [2] [3]. Many open source stereo matching algorithms have been developed. OpenCV has an algorithm for dense, area-based stereo matching, the block matching (BM) algorithm [4]. Another popular open-source, dense algorithm for real time stereo vision is the Efficient Large-Scale Stereo Matching (ELAS) algorithm [5]. While both of these algorithms are considered to be sufficient for real-time applications, the BM algorithm has been shown to be more efficient, while also maintaining sufficient accuracy for real-time applications [6]. One significant problem in real world contexts for stereo matching is the problem of finding stereo correspondences in areas of the images with homogeneous texture content [7]. This problem is intensified for algorithms that are optimized for speed and use limited computational power.

To solve the stereo correspondence problem, the field of active stereo vision has been explored, where a projection system illuminates the surface of a scene, adding distinct features that aid the stereo algorithm in finding correspondences. For example, scene reconstruction has been completed with the simple pattern of vertical black and white stripes projected with a standard projector [8]. A colored stripe, rainbow-like projection has also been attempted successfully [9] [10]. However, methods like these with standard projectors, such as DLP projectors, suffer from problems of interference with other sensors and high power usage. However, another type of projection system has been proposed that can address all of these problems experienced by traditional projectors: a laser speckle projection [11]. By projecting an objective speckle pattern using a laser system, distinct correspondences can be found in an image pair, allowing accurate 3D reconstruction. A laser speckle projection system has recently been applied successfully for measurements in medical applications [12]. The laser system can be inexpensive, compact, lightweight, and require well under a watt of power. Consequently, using an active stereo vision system with a laser speckle projector could be a successful sensor solution to the hitching problem.

Active Stereo Vision System Development

Coherent light sources, such as lasers, experience the phenomenon of interference, which is the principle that underlies the proposed laser speckle pattern projection. When a laser beam propagates through a rough surface, an objective interference pattern is generated. In practice, this can be achieved by passing the beam through a diffuser, which is an optical element that scatters light that is transmitted through it. A pattern of random speckles projected on a screen can be defined statistically by the average speckle size

$$\sigma_0 \cong \frac{1.2\lambda L}{D}, \tag{1}$$

where λ is the wavelength of the beam, L is the distance from the diffuser to the screen, and D is the diameter of the beam at the diffuser. The average speckle size σ_0 is defined as the average distance between regions of maximum and minimum brightness [13]. In order to increase the size of the spread of the projection and

also influence the size of the speckles created by the projection, a lens can be utilized to focus the beam onto the diffuser.

In the proposed setup, an inexpensive 650 nm laser diode was used which had a power of 50 mW. In order to greatly increase the intensity of the speckle pattern while still using a low-power, compact laser, long-pass optical filters were placed on the cameras in the stereo system. The filters have a cut-on wavelength of 645 nm. This specific filter was chosen for its low cost and because it transmits at least 75% of light at wavelengths of 650 nm or longer, while transmitting less than 5% of light at wavelengths of less than 620 nm, resulting in increased intensity of the speckle pattern. With the laser speckle system able to project onto a scene, it can be used in coordination with two cameras for active stereo vision. Each captured image pair from the two cameras can be used to reconstruct the scene in 3D by applying a stereo matching algorithm, and with the addition of the laser speckle projector, the system can accurately measure surfaces with homogeneous texture.

Mathematically, it is important to properly and accurately model the cameras within the system prior to calibration. The most widely used model is the pinhole model [4]. According to the pinhole camera model, a camera is mathematically described by

$$s\begin{bmatrix} u_i \\ v_i \\ 1 \end{bmatrix} = \boldsymbol{A}\begin{bmatrix} X^c \\ Y^c \\ Z^c \\ 1 \end{bmatrix} = \boldsymbol{A}[\boldsymbol{R}|\boldsymbol{T}]\begin{bmatrix} X^w \\ Y^w \\ Z^w \\ 1 \end{bmatrix}, \quad (2)$$

where s is a scaling factor, u_i and v_i define the image pixel coordinates, $\boldsymbol{A}$ is a matrix of intrinsic parameters, $\boldsymbol{R}$ is the rotation matrix between the camera coordinates and the world coordinates, and $\boldsymbol{T}$ is the translation vector between the camera coordinates and the world coordinates. $\boldsymbol{R}$ and $\boldsymbol{T}$ are considered the extrinsic parameters.

Calibration can then be completed to find the intrinsic and extrinsic parameters. Camera calibration by capturing many poses of a calibration board is well-studied. For high accuracy of the calibration, Zhang proposed using a circle pattern board for the calibration [14]. Precise identification of the circle centers can be achieved using OpenCV. Following identification of the circle centers in the images, OpenCV algorithms can be used to find the intrinsic parameters of the camera, and for many pairs of images from both cameras, the extrinsic parameters can be found [4].

After calibration, a stereo matching algorithm can be utilized to obtain a disparity image from the dual camera images. The block matching algorithm was chosen as the best option for this application. The algorithm was implemented using the OpenCV *StereoBM* class [4]. The block matching algorithm requires rectified images to work properly where matching stereo correspondences are mapped to be on the same rows of the images. This transformation is made possible geometrically by the existence of epipolar lines. With the extrinsic and intrinsic parameters known following calibration, the image can be remapped so that the epipolar lines in both the left and right image lie on the same horizontal row of pixels. This mapping is able to be completed using the OpenCV functions *stereoRectify*, *initUndistortRectifyMap*, and *remap* [4].

Once rectification has been completed, the block matching algorithm can be used. The fundamental principle of the block matching algorithm is minimizing the sum of absolute differences (SAD) between blocks of pixels on two images. For a pixel in the rectified left image, Lr, the SAD is computed as

$$SAD_k(u,v) = \sum_{m=u-L}^{u+L} |Lr(m,v) - Rr(m-k,v)| \quad (3)$$

for a linear horizontal window of size $2L + 1$ centered around pixel (u, v) compared to a window of the same size that scans the same row v on the rectified right image, Rr, where k can be incremented to scan one row of Rr. The minimum result will correspond to the matching pixel in the second image. The difference in column number of the matched pixels in the rectified images is the value of the disparity, σ. The results are stored in a disparity map.

One of the most significant problems with the standard block matching algorithms is that the disparity map only includes integer disparities. The issue with this is that it results in a large depth resolution, making precise object reconstruction impossible. Consequently, a sub-pixel algorithm developed by McCormick has been adapted for increased accuracy [15].

The principle of this algorithm is similar to the block matching algorithm. For a given pixel at location (u, v) in the rectified left image, a square block centered on that pixel is compared by sum of absolute differences with blocks centered on the same row in the rectified right image. Using the known integer disparity from the block matching algorithm, the only three pixels in the rectified right image that need their surrounding windows to be compared with the pixel of interest in the left image are the pixel corresponding exactly to the disparity found in block matching, and the pixel on its left and right, as shown in Figure 1. Importantly, to avoid adverse effects from using a rectangular window, the sum of absolute differences can be attenuated by a 2D Hann window, which is defined as

$$w(m,n) = 0.25\left(1 + \cos\left(\frac{\pi m}{L}\right)\right)\left(1 + \cos\left(\frac{\pi n}{L}\right)\right), \quad (4)$$

where m = *-L, -L + 1, … , 0, …, L-1, L* and n = *-L, -L + 1, …, 0, …, L - 1, L*, is used, smoothing out some artifacts present in the sub-pixel disparity map when no window, effectively a rectangular window, was used. Quadratic interpolation can then be used to find the sub-pixel disparity. The three points are fit with a quadratic curve, and the minimum of the curve is the sub-pixel disparity following

$$\delta = \sigma - \frac{(SAD_1(u,v) - SAD_{-1}(u,v))}{2(SAD_{-1}(u,v) - 2SAD_0(u,v) + SAD_1(u,v))}, \quad (5)$$

where δ is the subpixel disparity and σ is the integer disparity. $SAD_0(u,v)$, $SAD_{-1}(u,v)$, and $SAD_1(u,v)$ correspond to the sums of absolute differences of windows around the minimum pixel in the rectified right image and the pixels on its left and right, respectively, which can be computed as

$$SAD_{k-\sigma}(u,v) = \sum_{m=u-L}^{u+L}\sum_{n=v-L}^{v+L} \left|\left(Lr(m,n) - Rr(m-k,n)\right)\right|, \quad (6)$$

where the window of size $(2L + 1) \times (2L + 1)$ is centered at pixel (u, v) in the rectified left image Lr and compared to a window in the rectified right image Rr, and k being set to -1, 0, or 1.

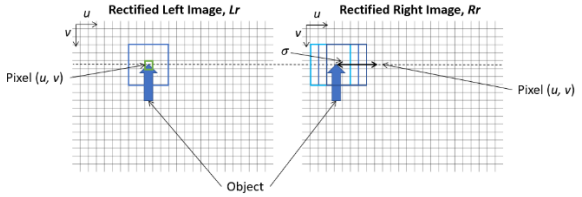

Figure 1. *Three square windows in the rectified right image compared to a square window in the left image for sub-pixel block matching.*

Overall, this algorithm increased both the accuracy and visual appearance of the results, and also was instrumental in implementing the algorithm in the real-time application.

3D reconstruction of the scene can be computed using the disparity values and the calibrated parameters through

$$K\begin{bmatrix} X^w \\ Y^w \\ Z^w \\ 1 \end{bmatrix} = \boldsymbol{Q}\begin{bmatrix} u \\ v \\ d \\ 1 \end{bmatrix} = \begin{bmatrix} 1 & 0 & 0 & -u_0 \\ 0 & 1 & 0 & -v_0 \\ 0 & 0 & 0 & f \\ 0 & 0 & -\frac{1}{T_x} & \frac{u_0 - u_0'}{T_x} \end{bmatrix}\begin{bmatrix} u \\ v \\ \delta \\ 1 \end{bmatrix}, \quad (7)$$

where the 4×4 $\boldsymbol{Q}$ matrix consists of known parameters from the calibration, u and u are the coordinates of the pixel with disparity δ [4]. Notably, u_0 and v_0 are defined for the left camera, while u_0' is defined for the right camera. T_x is the baseline length, which is the magnitude of the right camera translation matrix $\boldsymbol{T}$.

For object identification, it is important to have RGB texture data that can map to the measured 3D geometry. However, the two cameras in the stereo system have no meaningful color data, as the speckle pattern dominates the image, and most of the color content is filtered out by the optical filters. Consequently, a third camera is proposed that can map the RGB texture from the scene to the measured geometry. This camera is calibrated with respect to the left camera in the stereo vision system. This camera is covered with a short-pass optical filter, so the red laser light is filtered out.

In order to map the color data with the 3D geometry that has already been computed, the pinhole camera model from Equation (2) can be used. With the world coordinates known, and all the intrinsic and extrinsic parameters known for the texture camera, Equation (2) can be solved for the pixel in the texture image that corresponds to that specific world coordinate. As a result, the texture content can be accurately mapped to the 3D geometry.

The accuracy of the sensor was evaluated first by measuring a sphere with a radius of 15 cm. In this experiment, the effect of applying the subpixel matching algorithm was tested, as well as the effect of projecting a second speckle pattern onto the sphere, in order to ensure that interference between multiple sensors was not a problem. Each measurement was reconstructed to 3D, and the best fit sphere was computed. Figure 2 shows one of the measurements taken with a single speckle pattern projection with a camera resolution of 1280 × 720, including the left and right images in Figure 6 (a)-(b), the disparity map in Figure 2 (c), and the 3D reconstruction from integer disparity and sub-pixel disparity in Figure 2 (d)-(e).

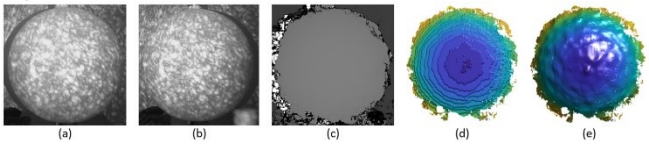

Figure 2. *Measurement of a sphere at a camera resolution of 1280×720 on which a single speckle pattern is projected. (a) Left image; (b) Right image; (c) Disparity map; (d) 3D reconstruction from integer disparity map; (e) 3D reconstruction from sub-pixel disparity map.*

In order to characterize the error, spheres were measured at distances ranging from 0.75 m to 1.5 m. For each measurement, the root mean squared error (RMSE) was calculated for the measured area of the sphere, where a point in the point cloud is a distance r_n away from the center of the best fit sphere of radius r, and N such points are used in the measurement. Tests were completed at the camera resolutions of 320 × 240, 640 × 480, and 1280 × 720, and for each test a single speckle pattern was used for one measurement and a double speckle pattern was used for a second measurement. Furthermore, for the single speckle pattern the integer disparity was also tested without using the sub-pixel matching algorithm to evaluate the value added from implementing the algorithm. The results for this experiment are collected in Figure 3.

It can be seen that the sub-pixel matching algorithm significantly improves the measurement in comparison with the block matching algorithm, which yields integer disparity values. For the twelve tests in Figure 3, the RMSE is an average of 1.9 times worse if the sub-pixel matching is not applied. There is only a minor effect on the error from adding a second speckle pattern projection on the sphere, as the average increase in RMSE from a single speckle pattern to a double speckle pattern is 0.14 mm. Finally, the resolution improvement from 320 × 240 to 640 × 480 in Figure 3 (a)-(b) yields a decrease in error by a factor of 1.3. The increase in resolution from 640 × 480 to 1280 × 720 in Figure 3 (b)-(c) improves the accuracy by a factor of 1.6.

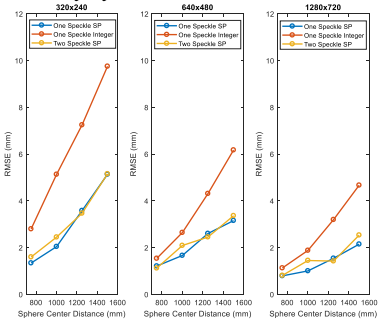

Figure 3. *Root mean squared error results for tests at distances between 0.75m and 1.5m and using a single speckle pattern as well as two speckle pattern projections. The single speckle projection is evaluated using both a 3D reconstructed integer disparity map and a 3D reconstructed sub-pixel disparity map. (a) 320 × 240 resolution; (b) 640 × 480 resolution; (c) 1280 × 720 resolution.*

Autonomous Vehicle Control Experiments

In order to model the hitching problem, an object representing a hitch was designed. This target object is shown in Figure 4 and has similar features to a standard agricultural three-point hitch. The target was 3D printed to rapidly test the design.

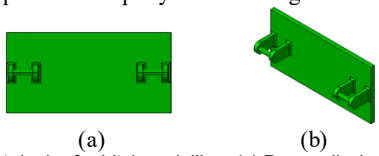

Figure 4. *Target design for hitch modelling. (a) Perpendicular view; (b) Isometric view.*

The model vehicle for this work is the Traxxas Slash 2WD vehicle. This vehicle is large enough to easily fit the cameras, mobile computer, and various batteries and other components on the vehicle. One critical feature of this vehicle is that each wheel has its own suspension, making it a good model for an agricultural vehicle that is designed to be able to navigate rough terrain. The vehicle is also able to drive in reverse, which is crucial for hitching. We define the dynamics of the vehicle using the common bicycle model for a vehicle with three degrees of freedom, which simplifies the vehicle dynamics [16]. Using this model, the stable control system proposed by Kanayama et al. is implemented in order to control the vehicle position and angle [17].

In the application, it is desired for the vehicle to approach the target perpendicularly. Consequently, the reference, or desired values, so the measured value of these parameters is also the error. The control scheme can then be described by

$$\omega(K_y, K_\theta) = \omega_r + v_r(K_y y + K_\theta \sin(\theta)), \quad (11)$$

where the position of the vehicle in Cartesian coordinates is given by x and y, the vehicle angle is given by θ, the angle of the wheel is the parameter ω, and the speed of the vehicle is defined as v. K_y and K_θ are constant control parameters and ω_r is the feedforward wheel angle, which is set to zero since the desired path is a straight line perpendicular to the target [17].

It is next needed to find the target using the texture camera in order to sense it. A process of color thresholding, erosion, and dilation proved to be robust, and can be visualized in Figure 5, which also shows how the algorithm is robust to other objects of similar shades of color to the target.

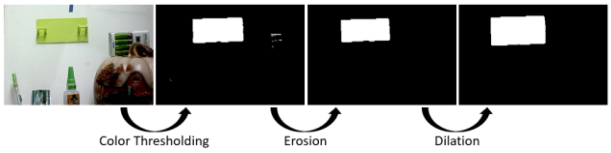

Figure 5. *Example scene demonstrating algorithms used for target identification.*

The corners of the target were then found with a process that used OpenCV *findContours,* to find the contour of the binary image, which was then approximated as a quadrilateral using the Douglas-Peucker algorithm [4] [18], and the corners can then be refined using the *cornerSubPix* algorithm on the grayscale image [4].

By using the corner locations along with the texture camera intrinsic calibration, it is possible to identify the position and orientation of the target. While this method is less accurate than stereo vision at short distances, it is accurate enough for control of the vehicle at far distances where the stereo vision is less reliable. To solve this, the *EPnP* method has been incorporated using the *solvePnP* OpenCV algorithm [4] [19].

It is also possible for the stereo vision block matching algorithm to be incorporated in order to find the position and orientation of the target more precisely using the stereo vision cameras. Notably, the stereo camera resolution is set to 320 × 240 in order to maximize speed while still having sufficient accuracy. With the target found using the texture camera, the stereo camera can calculate the target position.

In controlling the vehicle precisely, it is important for the stereo camera to not only calculate the position of the target, but also its angular orientation. However, the raw 3D reconstruction of integer disparity values is insufficient for any angular calculation, due to the insufficient depth resolution. In looking at the target, it can be recognized that the angle of the target can be found by finding the angle of a line of pixels within the flat area of the target. After reconstructing a horizontal line of pixels on the target to a 3D point cloud, the best fit line can be calculated. The analysis can be simplified by only considering one plane parallel to the floor. This is possible since only the angular rotation with respect to this plane is relevant to the vehicle control. The slope of the best fit line with n points in the $X^W - Z^W$ plane is defined as

$$m = \frac{n*(\sum_{i=1}^{n} x_i * z_i) - (\sum_{i=1}^{n} x_i)(\sum_{i=1}^{n} z_i)}{n*(\sum_{i=1}^{n} x_i^2) - (\sum_{i=1}^{n} x_i)^2}, \quad (14)$$

The arctangent of the slope is the angle of the line in radians with respect to the Z^c axis of the left camera, described mathematically as

$$\alpha = \tan^{-1} m, \quad (15)$$

By averaging the angle calculated from several lines the noise of the measurement can be reduced to a stable signal that can be used as a controller input, yet the processing power required for sub-pixel matching can be minimized.

With the vision system developed and incorporated onto the vehicle and a control system adapted to precisely control the vehicle, the entire system can be examined through testing. The testing is done starting at 1.5 m between -15º and +15º of the perpendicular line of the vehicle.

The angle of the target is able to be sensed from the texture camera, or from the stereo camera. At larger distances the angle measurement from the texture camera was found to be less noisy than that of the stereo camera. Between 1.15 and 1.5 m, the single camera measurement was used for the angular signal. When under 1.15 m, stereo vision was used to measure the target angle. Regardless of distance, the stereo vision was used to measure the distance from the target.

The system was tested by starting the vehicle at seven different starting angles of approach, and then measuring the final orientation of the vehicle after it stopped, with six tests performed for each angle of approach. The vehicle started at a distance of 1.5 m from the target in these tests, which is the distance at which a far distance control system that has been developed for the vehicle can reliably deliver the vehicle to within ±15º. The test results are given in Table 1, showing the vehicle starting angle from the target, the mean final measurement error for each angle of approach, and the standard deviation of that measurement error across the six tests at that angle of approach. Furthermore, based upon the mean results from each angle, a standard deviation is given, as well as a standard deviation across all 42 tests.

Table 1. Final vehicle testing results.

Starting Angle of Approach (°)	x error (mm), mean, std. dev.	y error (mm), mean, std. dev.	θ error (°), mean, std. dev.
-15	-0.8, 2.5	12.3, 1.5	2.1, 0.38
-10	0.0, 1.5	13.3, 2.4	1.4, 0.86
-5	-0.3, 1.6	10.0, 2.8	0.4, 0.38
0	1.0, 3.7	12.3, 2.4	0.1, 0.66
5	0.0, 2.3	12.2, 3.4	-0.6, 0.58
10	-1.3, 2.0	10.8, 4.0	-1.0, 1.10
15	-0.2, 1.2	8.3, 1.2	-2.0, 0.32
Std. dev. of means of each angle of approach	0.7	1.7	1.4
Std. dev. of all 42 tests	2.2	3.0	1.5

Overall for all the tests, the lateral standard deviation was found to be 3.0 mm and the angular standard deviation was found to be 1.5º, which characterizes the overall spread of the error, irrespective of the starting position.

Summary

In this paper, a sensor solution has been developed to tackle the autonomous hitching problem, and the system has been tested on a model vehicle. The sensor is stereo vision based, and solves the stereo correspondence problem with a laser speckle projection system. The sensor far exceeds any proven solutions in existing technology and literature, as the total cost is just $188, the power requirement is 2.3 W, and no modification to the hitch is required for sensing. In the testing of a model system, the model vehicle was shown to have an angular error of 1.5º, with a lateral approach error of 3.0 mm.

References

[1] T. Ahamed, L. Tian, T. Takigawa and Y. Zhang, "Development of Auto-Hitching Navigation System for Farm Implements Using Laser Range Finder," Transactions of the ASABE, vol. 52, no. 5, pp. 1793-1803, 2009.T. Jones, "Sample Journal Article," Jour. Imaging Sci. and Technol., vol. 53, no. 1, pp. 1-5, 2009.

[2] N. Lazaros, G. Sirakoulis and A. Gasteratos, "Review of Stereo Vision Algorithms: From Software to Hardware," International Journal of Optomechatronics, vol. 2, no. 4, pp. 435-462, 2008.

[3] R. Hamzah and H. Ibrahim, "Literature Survey on Stereo Vision Disparity Map Algorithms," Journal of Sensors, vol. 2016, 2016.

[4] G. Bradski and A. Kaehler, Learning OpenCV, O'Reilly Media, Inc., 2008.

[5] A. Geiger, M. Roser and R. Urtasun, "Efficient Large-Scale Stereo Matching," in Computer Vision – ACCV 2010, 2010.

[6] X. Hu, Y. Wu, D. Zhang, L. Qian and L. Wu, "Research on Improvement of Stereo Matching Algorithm," Journal of Computers, vol. 19, no. 4, pp. 110-121, 2018.

[7] M. Brown, D. Burschka and G. Hager, "Advances in Computational Stereo," IEEE Transactions on Pattern Analysis and Machine Intelligence, vol. 25, pp. 993-1008, 2003.

[8] J. Diebel, K. Reuterswad, S. Thrun, J. Davis and R. Gupta, "Simultaneous Localization and Mapping with Active Stereo Vision," in Proceedings of 2004 IEEE/RSJ International Conference on Intelligent Robots and Systems, Sendal, Japan, 2004.

[9] A. Koschan, V. Rodehorst and K. Spiller, "Color Stereo Vision Using Hierarchical Block Matching," in Proceedings of 13th International Conference on Pattern Recognition, Vienna, Austria, 1996.

[10] W. Jang, C. Je, Y. Seo and S. Lee, "Structured-light stereo: Comparative analysis and integration of structured-light and active stereo for measuring dynamic shape," Optics and Lasers in Engineering, vol. 51, no. 11, pp. 1255-1264, 2013.

[11] M. Schaffer, M. Grosse and R. Kowarschik, "High-speed pattern projection for three-dimensional," Applied Optics, vol. 49, no. 18, pp. 3622-3629, 2010.

[12] D. Khan, M. Shirazi and M. Kim, "Single shot laser speckle based 3D acquisition system for medical applications," Optics and Lasers in Engineering, vol. 105, pp. 43-53, 2018.

[13] J. Dainty, Laser Speckle and Related Phenomena, New York: Springer-Verlag Berlin Heidelberg, 1975.

[14] S. Zhang, High-speed 3D imaging with digital fringe projection techniques, CRC Press, Taylor & Francis Group LLC, 2016.

[15] C. McCormick, "Stereo Vision Tutorial - Part I," January 2014. [Online]. Available: http://mccormickml.com/2014/01/10/stereo-vision-tutorial-part-i/. [Accessed August 2019].

[16] J. Laumond, S. Sekhavat and F. Lamiraux, Guidelines in Nonholonomic Motion Planning for Mobile Robots, Springer, Berlin, Heidelberg, 1998.

[17] Y. Kanayama, Y. Kimura, F. Miyazaki and T. Noguchi, "A stable tracking control method for an autonomous mobile robot," in Proceedings., IEEE International Conference on Robotics and Automation, Cincinnati, 1990.

[18] D. Douglas and T. Peucker, "Algorithms for the reductions of the number of points required to represent a digitised line or caricature," The Canadian Cartographer, vol. 10, no. 2, pp. 112-122, 1974.

[19] V. Lepetit, F. Moreno-Noguer and P. Fua, "EPnP: An Accurate O(n) Solution to the PnP Problem," International Journal of Computer Vision, vol. 81, 2009.

Author Biography

Michael Feller received his Master's degree in Mechanical Engineering in December 2019 while working with Professor Song Zhang. Michael has interests in optics, robotics, and vehicle control. He currently works developing ADAS algorithms as a software engineer for Ford Motor Company.

Jae-Sang Hyun is a Ph.D. candidate working with Professor Song Zhang in School of Mechanical Engineering at Purdue University. He received his Master's degree from Purdue University in 2019. His research interests are three-dimensional optical metrology, machine vision, robotics, and embedded system.

Song Zhang is a Professor of mechanical engineering at Purdue University. He received his Ph.D. degree from Stony Brook University in 2005. His current research interests include 3-D machine/computer vision, autonomous vehicles, virtual reality, augment vision, forensic science, and biomedical engineering. He has authored or co-authored over 200 research articles. He serves as an Associate Editor for Optics and Lasers in Engineering, and a Technical Editor for IEEE/ASME Transactions on Mechatronics. He is a fellow of SPIE and OSA.

JOIN US AT THE NEXT EI!

IS&T International Symposium on

Electronic Imaging

SCIENCE AND TECHNOLOGY

Imaging across applications . . . Where industry and academia meet!

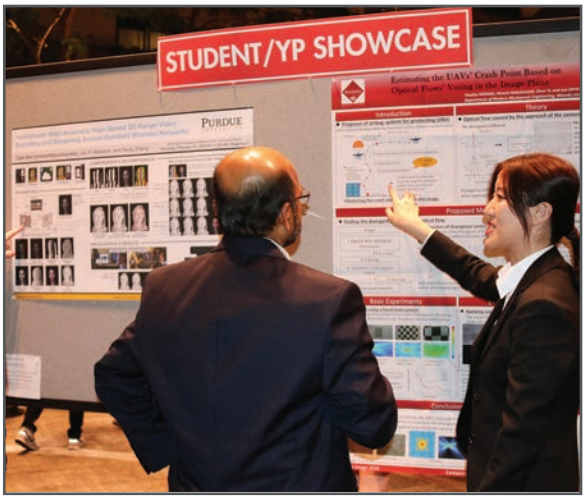

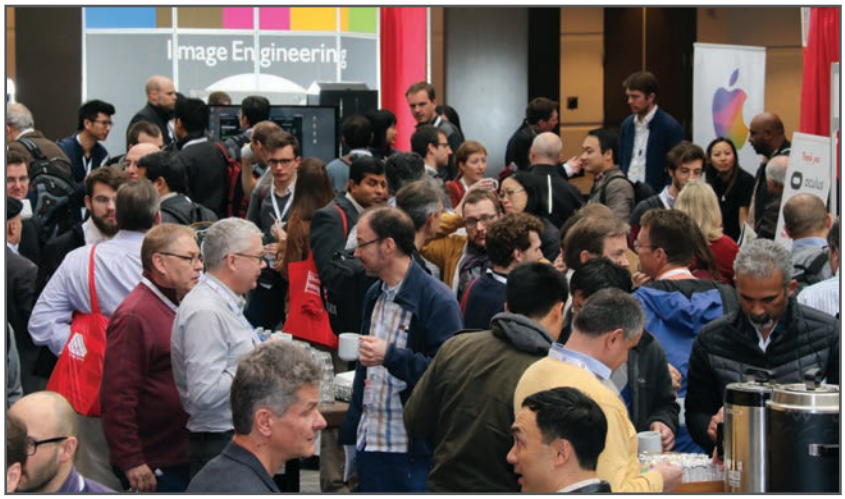

• SHORT COURSES • EXHIBITS • DEMONSTRATION SESSION • PLENARY TALKS •
• INTERACTIVE PAPER SESSION • SPECIAL EVENTS • TECHNICAL SESSIONS •

www.electronicimaging.org

IS&T
imaging.org